J. Appl. Comput. Mech., 6(2) (2020) 357-372
DOI: 10.22055/JACM.2019.29527.1609

ISSN: 2383-4536
jacm.scu.ac.ir

M&MoCS

Shahid Chamran University of Ahvaz

Journal of Applied and Computational Mechanics

Research Paper

An Analytical Approach of Nonlinear Thermo-mechanical Buckling of Functionally Graded Graphene-reinforced Composite Laminated Cylindrical Shells under Compressive Axial Load Surrounded by Elastic Foundation

**Ngoc Ly Le[1], Thi Phuong Nguyen[2], Hoai Nam Vu[3,4], Thoi Trung Nguyen[3,4]
Minh Duc Vu[2]**

[1] Faculty of Fundamental Science for Engineering, University of Transport Technology, Hanoi, 100000, Vietnam

[2] Faculty of Civil Engineering, University of Transport Technology, Hanoi, 100000, Vietnam

[3] Division of Computational Mathematics and Engineering, Institute for Computational Science, Ton Duc Thang University, Ho Chi Minh City, 700000, Vietnam

[4] Faculty of Civil Engineering, Ton Duc Thang University, Ho Chi Minh City, 700000, Vietnam

Received May 13 2019; Revised July 28 2019; Accepted for publication August 06 2019.
Corresponding author: Hoai Nam Vu (vuhoainam@tdtu.edu.vn)

Abstract. This paper deals with an analytical approach to predict the nonlinear buckling behavior of functionally graded graphene-reinforced composite laminated cylindrical shells under axial compressive load surrounded by Pasternak's elastic foundation in a thermal environment. Piece-wise functionally graded graphene-reinforced, composite layers are sorted with different types of graphene distribution. The governing equations are established by using Donnell's shell theory with von Kármán nonlinearity terms and three-term solution of deflection is chosen for modeling the uniform deflection of pre-buckling state, linear and nonlinear deflection of post-buckling state. Galerkin method is applied to determine the critical axial compressive buckling load expression, post-buckling load-deflection and load-end shortening relations of the shell. The effects of environment temperature, foundation, geometrical properties, and graphene distribution on buckling behavior of shell, are numerically evaluated.

Keywords: Functionally graded graphene-reinforced composite; cylindrical shell; compressive axial load; thermo-mechanical buckling; elastic foundation.

1. Introduction

Cylindrical shells are one of the major load-bearing components in an airplane, civil engineering, nuclear reactors, and other important engineering structures. In recent year, many authors are mostly interested in the linear and nonlinear buckling and post-buckling behavior of cylindrical shells made by different materials.

Elastic and inelastic mechanical buckling behavior of isotropic and traditional composite, cylindrical shells were mentioned in many works. Shen et al. [1] studied the post-buckling response of stiffened isotropic cylindrical shells subjected to external pressure and axial compressive load by using a singular perturbation technique and a boundary layer theory taking into account the edge effect and geometrical imperfection of shells. Reddy and Starnes [2] proposed a general buckling approach of stiffened circular cylindrical shells reinforced by axial and circumferential stiffeners. The

Published online: September 05 2019

layerwise theory and Navier's solution were developed for the buckling behavior of shells. Postbuckling behavior of perfect and imperfect stiffened laminated circular cylindrical shells of finite length subjected to combined external pressure and axial compression was investigated by Shen [3]. Mandal and Calladine [4] studied the self-weight buckling of open-top, fixed-base, small-scale silicone rubber circular cylindrical shells under axial compressive load by using the simple experiments. Lancaster et al. [5] investigated the effect of imperfections on the buckling load in the form of local initial stress of circular cylindrical shells. The unexpected and paradoxical features of the buckling behavior of imperfect shell were observed. Karagiozova and Jones [6] investigated the dynamic inelastic buckling behavior of cylindrical shells subjected to axial impact loads. Postbuckling behavior of stiffened braided circular cylindrical shells subjected to external pressure and axial compression with the nonlinear large deflection effect and the initial geometrical imperfection was studied by Zeng and Wu [7]. Theoretical estimation of bifurcation load for a collection of experiments data of axially compressive composite cylindrical shells by using the bi-modal and torsion solution and Galerkin procedure was reported by Biagi and Medico [8]. Tafreshi [9] studied the delaminated composite cylindrical shells subjected to bending and axial compressive load by using the finite element method with double-layer and single-layer shell elements. Li and Yang [10] investigated the nonlinear post-buckling behavior of stiffened fiber-reinforced thick laminated cylindrical shell of finite length subjected to axial compression by using the higher-order shear deformation theory. Cao et al. [11] investigated free vibration of orthotropic cylindrical shell with constrained layer damping based on the Rayleigh-Ritz energy method and Sanders' thin shell theory.

Functionally graded materials (FGMs) are the advanced composite materials in which thermomechanical properties are continuously varied through the thickness of the structure. From the continuous change in composition, FGM is popularly used as the heat-resistant materials. Shen [12] investigated the post-buckling analysis of FGM cylindrical shells in thermal environments subjected to axial compression by using the singular perturbation technique. Research on thermo-mechanical behavior of FGM structure has been an exciting field in the last decade. The modified Donnell shell theory and geometrical compatibility equations were used by Sofiyev and Schnack [13] to investigate the dynamic stability of FGM cylindrical shells under dynamic torsion load. By using the trigonometric function form, the linear buckling of the three-layer circular cylindrical shell under axial compressive load was reported by Li and Batra [14]. An analytical approach to investigate the linear and nonlinear buckling behavior of FGM cylindrical shells subjected to axial compressive load was mentioned by Huang and Han [15, 16]. Donnell shell theory, von Kármán nonlinearity type, Ritz energy method, and three-term solution form were applied and nonlinear post-buckling behavior of shell was obtained. Based on the Galerkin method, nonlinear buckling and post-buckling behavior of FGM cylindrical shells with a ring, stringer and spiral eccentrically stiffeners subjected to external pressure, axial compressive and torsional loads were studied [17-20]. Mehditabar et al. [21] studied the three-dimensional magneto-thermo-elastic behavior of FGM cylindrical shell in an applied thermal environment and magnetic fields subjected to non-uniform internal pressure. Sofiyev and Hui [22] studied the vibration and stability behavior of FGM thick cylindrical shells subjected to external pressure with mixed boundary conditions.

In recent years, carbon nanotubes (CNTs) have attracted more attention of many authors for their extraordinaire properties. Based on the idea of FGM, the CNTs are used to reinforce in the polymeric matrix, new material is formed, namely, functionally graded carbon nanotube-reinforced composite (FG-CNTRC). Song et al. [23, 24] investigated the vibration analysis of FG-CNTRC higher-order shear deformable cylindrical shells with or without piezoelectric patches. Hosseini and Kolahchi [25] investigated the viscoelastic dynamic response and damping effects of FG-CNTRC submerged cylindrical shell subjected to an earthquake in the hygrothermal environment.

Like CNTs, the graphene sheets can be used to reinforce in the polymer matrix to induce a new material with extraordinaire performance. On other hands, the better polymer matrix and graphene sheet interactions are obtained due to the high surface area of graphene sheets and its structure. By using the first-order shear deformation beam theory and von Kármán type of geometrical nonlinearity, Mirzaei and Kiani [26] studied the non-linear thermal stability of temperature dependent laminated beams with graphene reinforcements. Mirzaei and Kiani [27] and Kiani [28, 29] investigated the thermal buckling, free vibration and post-buckling behavior of functionally graded graphene reinforced composite (FG-GRC) laminated plates by using the non-uniform rational B-spline (NURBS) formulation. Buckling of FG-GRC conical shells under external pressure in thermal environment was studied by Kiani [30]. Shen et al. [31-33] investigated the nonlinear postbuckling, vibration and bending of functionally graded graphene reinforced composite laminated plates with plate-foundation interaction by using the two-step perturbation technique. With a similar approach, the post-buckling analysis of FG-GRC laminated cylindrical shells under axial compression and external pressure in the thermal environments by Shen and Xiang [34, 35]. Barati and Zenkour [36] investigated the vibration analysis of functionally graded graphene platelet reinforced cylindrical shells with uniform, symmetric, and asymmetric porosity distributions. By using the finite element method, Wang et al. [37] investigated eigenvalue buckling of functionally graded graphene platelet reinforced composite cylindrical shells. Zhenhuan et al. [38] proposed an accurate approach of nonlinear buckling behavior of functionally graded porous graphene platelet reinforced composite cylindrical shells.

In the present work, a simple and effective analytical approach of nonlinear buckling of FG-GRC laminated cylindrical shells is presented. The Donnell's shell theory with von Kármán nonlinearity, three-term solution type of deflection and the Galerkin method are applied to obtain the critical axial compressive buckling loads, post-buckling load-deflection and load-end shortening curves of FG-GRC laminated cylindrical shells surrounded by two-parameter Pasternak's elastic foundation in thermal environment. Effects of environment temperature, elastic foundation parameters, geometrical properties and graphene distribution type on the nonlinear buckling behavior of shell are numerically investigated and discussed.

2. FG-GRC Laminated Cylindrical Shells Surrounded by Elastic Foundation

Consider an FG-GRC laminated cylindrical shell subjected to an axial compressive load of uniform distribution intensity p with the mean radius R, the total thickness h, and the length L as shown in Fig. 1.

Each layer is made of a mixture of graphene reinforcement and the polymer matrix. The middle surface of shells is referred to the coordinates (x, y, z) in which x is chosen in the longitudinal direction, the coordinate axis y and z are in the circumferential and thickness directions of the shell, respectively.

The graphene reinforcement in the x axis direction is denoted by (0-layer) while the y axis direction is denoted by (90-layer). So each layer in the FG-GRC cylindrical shells structure has a different arrangement, divided into three samples of cylindrical shells $(0)_{10}$, $(0/90/0/90/0)_S$ and $(0/90)_{5T}$. Also, five different graphene distribution types, namely, UD, FG-X, FG-V, FG-Λ and FG-O are considered. The graphene volume fractions are gradually increased from inside layer to outside layer for FG-Λ distribution type and vice versa for FG-V distribution type, the ten layer of the two types are denoted by $[(0.11)_2/(0.09)_2/(0.07)_2/(0.05)_2/(0.03)_2]$ referred to as FG-Λ and $[(0.03)_2/(0.05)_2/(0.07)_2/(0.09)_2/(0.11)_2]$ referred to as FG-V. For FG-O, FG-X distribution types the five inside layers have graphene volume fractions distributed symmetrically with the five outside layers, $[0.11/0.09/0.07/0.05/0.03]_S$ referred to as FG-O distribution type and $[0.03/0.05/0.07/0.09/0.11]_S$ referred to as FG-X distribution type. For UD distribution type, the graphene volume fraction is distributed uniformly across all layers $(V_G = 0.07)$. According to the extended Halpin–Tsai model, the Young's moduli and the shear modulus of the FG-GRC layer are taken according to the work of Shen et al. [33].

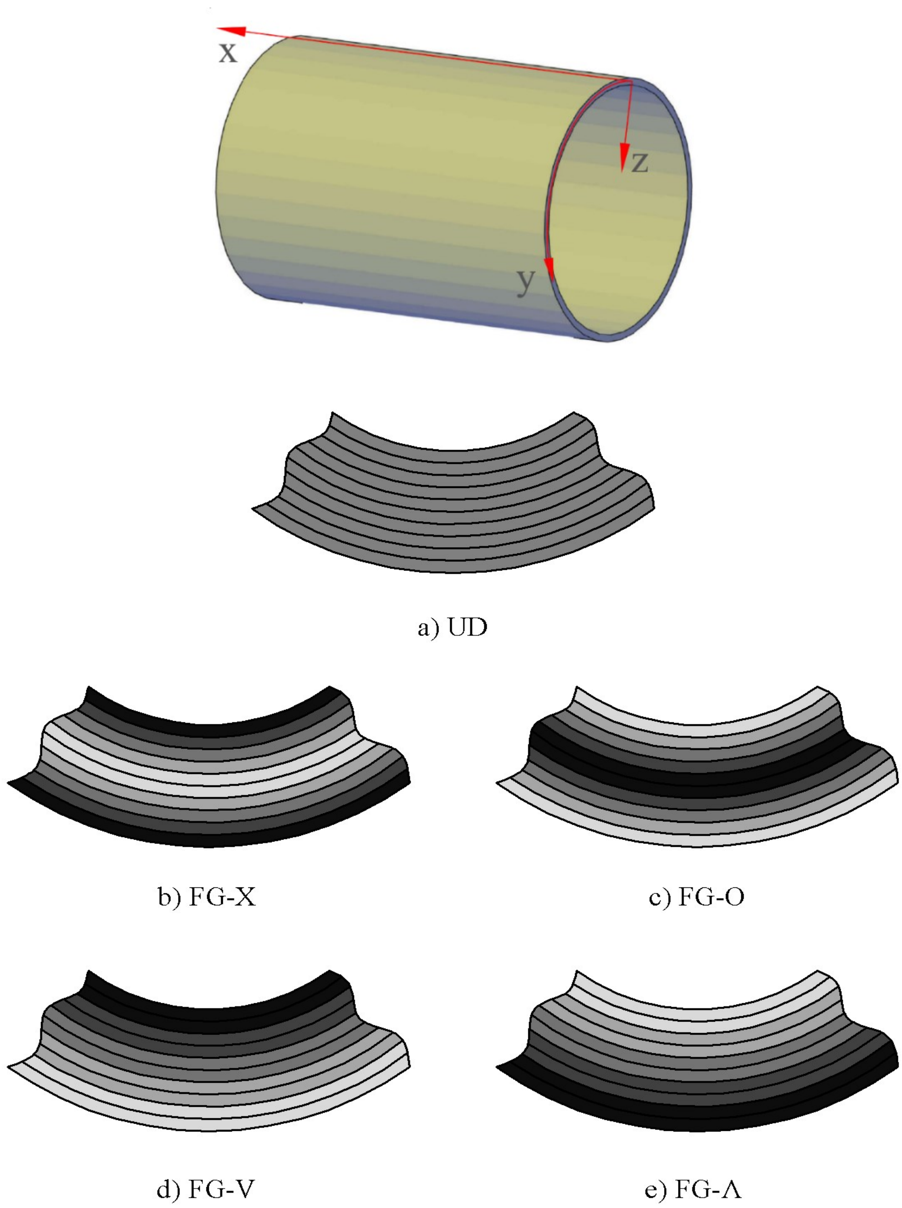

Fig. 1. Configuration and coordinate system of FG-GRC laminated cylindrical shell and graphene distribution types.

In this paper, the graphene sheets are distributed in the x direction, the orthotropic Young's moduli are written by

$$\begin{gathered} E_{11}=\eta_1\frac{1+2(a_G/h_G)\gamma_{11}^G V_G}{1-\gamma_{11}^G V_G}E^m, \\ E_{22}=\eta_2\frac{1+2(b_G/h_G)\gamma_{22}^G V_G}{1-\gamma_{22}^G V_G}E^m,\quad G_{12}=\eta_3\frac{1}{1-\gamma_{12}^G V_G}G^m, \end{gathered} \tag{1}$$

with

$$\begin{gathered} \gamma_{11}^G=\frac{E_{11}^G/E^m-1}{E_{11}^G/E^m+2a_G/h_G}, \\ \gamma_{22}^G=\frac{E_{22}^G/E^m-1}{E_{22}^G/E^m+2b_G/h_G},\quad \gamma_{12}^G=\frac{G_{12}^G/G^m-1}{G_{12}^G/G^m}, \end{gathered} \tag{2}$$

where a_G, b_G and h_G are the length, width and effective thickness of the graphene sheet, respectively. $(E^m,\ G^m)$ and $(E_{11}^G,\ E_{22}^G,\ G_{12}^G)$ are the orthotropic Young's moduli and shear moduli of the matrix and the graphene sheet, respectively. V_G and V_m are the graphene and matrix volume fractions, respectively, with the condition $V_G+V_m=1$. In Eq. (1), the graphene efficiency parameters η_j $(j=1,\ 2,\ 3)$ are taken according to the graphene volume fraction V_G in the Table 1.
The GRC layer have the thermal expansion coefficients in the x and y axis directions of the matrix and the graphene sheet are taken according to the work of Shen et al. [30]

$$\begin{gathered} \alpha_{11}=\frac{V_G E_{11}^G\alpha_{11}^G+V_m E^m\alpha^m}{V_G E_{11}^G+V_m E^m}, \\ \alpha_{22}=(1+\nu_{12}^G)V_G\alpha_{22}^G+(1+\nu^m)V_m\alpha^m-\nu_{12}\alpha_{11}, \end{gathered} \tag{3}$$

where α_{11}^G, α_{22}^G and α^m are the thermal expansion coefficients, ν_{12}^G and ν^m are the Poisson's ratios of the graphene sheet and the matrix, respectively. Here, the material properties are assumed to be $\nu^m=0.34$, $\alpha^m=45(1+0.0005\Delta T)\times10^{-6}/K$ and $E^m=(3.52-0.0034T)\ GPa$, in which $T=T_0+\Delta T$ and $T_0=300K$ (room temperature). The Poisson's ratio of GRCs depends heavily on environment temperature and is denoted by

$$\nu_{12}=V_G\nu_{12}^G+V_m\nu^m. \tag{4}$$

The thermomechanical properties of graphene sheet as given in Eqs. (1) and (3) are derived by Shen et al. [33]

$$\begin{aligned} &\nu_{12}^G=0.177, \\ &E_{11}^G=(2.16637-0.00193T+2.93701\times10^{-6}T^2-1.51775\times10^{-9}T^3)TPa, \\ &E_{22}^G=(2.16868-0.00193T+2.85954\times10^{-6}T^2-1.45145\times10^{-9}T^3)TPa, \\ &G_{12}^G=(0.53514+8.24436\times10^{-4}T-1.2932\times10^{-6}T^2+5.78507\times10^{-10}T^3)TPa, \\ &\alpha_{11}^G=(-3.83788+0.01416T-1.63355\times10^{-5}T^2+6.33589\times10^{-9}T^3)\times10^{-6}/K, \\ &\alpha_{22}^G=(-3.73997+0.01296T-1.35033\times10^{-5}T^2+4.60392\times10^{-9}T^3)\times10^{-6}/K. \end{aligned} \tag{5}$$

3. Governing Equations

In the present research, the Donnell shell theory is used to establish the fundamental equations for buckling and nonlinear analysis of FG-GRC laminated cylindrical shells subjected to uniform axial compression in thermal environments. The strains across the cylindrical shell thickness at a distance z from the middle surface are written by

$$\begin{bmatrix}\varepsilon_x\\ \varepsilon_y\\ \gamma_{xy}\end{bmatrix}=\begin{bmatrix}\varepsilon_x^0\\ \varepsilon_y^0\\ \gamma_{xy}^0\end{bmatrix}-z\begin{bmatrix}\chi_x\\ \chi_y\\ 2\chi_{xy}\end{bmatrix}, \tag{6}$$

Table 1. The performance parameters of graphene/PMMA nanocomposites [33]

$T(K)$	V_G	η_1	η_2	η_3
300	0.03	2.929	2.855	11.842
	0.05	3.068	2.962	15.944
	0.07	3.013	2.966	23.575
	0.09	2.647	2.609	32.816
	0.11	2.311	2.260	33.125
400	0.03	2.977	2.896	13.928
	0.05	3.128	3.023	15.229
	0.07	3.060	3.027	22.588
	0.09	2.701	2.603	28.869
	0.11	2.405	2.337	29.527
500	0.03	3.388	3.382	16.712
	0.05	3.544	3.414	16.018
	0.07	3.462	3.339	23.428
	0.09	3.058	2.936	29.754
	0.11	2.736	2.665	30.773

where ε_x^0 and ε_y^0 are normal strains, γ_{xy}^0 is the shear strain at the middle surface of shell, and

$$\begin{bmatrix}\varepsilon_x^0\\ \varepsilon_y^0\\ \gamma_{xy}^0\end{bmatrix}=\begin{bmatrix}u_{,x}+w_{,x}^2/2\\ v_{,y}-w/R+w_{,y}^2/2\\ u_{,y}+v_{,x}+w_{,x}w_{,y}\end{bmatrix},\quad \begin{bmatrix}\chi_x\\ \chi_y\\ \chi_{xy}\end{bmatrix}=\begin{bmatrix}w_{,xx}\\ w_{,yy}\\ w_{,xy}\end{bmatrix}, \tag{7}$$

where von Kármán–Donnell nonlinearity terms are considered, $u=u(x,y)$, $v=v(x,y)$, $w=w(x,y)$ are displacements along x, y and z directions, respectively
Deformation compatibility equation is received from Eq. (7), as

$$\varepsilon_{x,yy}^0+\varepsilon_{y,xx}^0-\gamma_{xy,xy}^0=-\frac{1}{R}w_{,xx}+w_{,xy}^2-w_{,xx}w_{,yy}. \tag{8}$$

Stress–strain relations of Hooke law for FG-GRC laminated cylindrical shell are written by

$$\begin{bmatrix}\sigma_x\\ \sigma_y\\ \sigma_{xy}\end{bmatrix}=\begin{bmatrix}Q_{11} & Q_{12} & 0\\ Q_{12} & Q_{22} & 0\\ 0 & 0 & Q_{66}\end{bmatrix}\left(\begin{bmatrix}\varepsilon_x\\ \varepsilon_y\\ \gamma_{xy}\end{bmatrix}-\begin{bmatrix}\alpha_{11}\\ \alpha_{22}\\ 0\end{bmatrix}\Delta T\right), \tag{9}$$

where

$$Q_{11}=\frac{E_{11}}{1-\nu_{12}\nu_{21}},\ Q_{22}=\frac{E_{22}}{1-\nu_{12}\nu_{21}},\ Q_{12}=\frac{\nu_{21}E_{11}}{1-\nu_{12}\nu_{21}},\ Q_{66}=G_{12},$$

and ΔT is the uniform distribution temperature change with respect to a reference state. The force and moment of a FG-GRC laminated cylindrical shell are shown in terms of the stress components through the thickness as

$$\left(N_x, N_y, N_{xy}\right)=\int_{\frac{-h}{2}}^{\frac{h}{2}}\left(\sigma_x, \sigma_y, \sigma_{xy}\right)dz,\ \left(M_x, M_y, M_{xy}\right)=\int_{\frac{-h}{2}}^{\frac{h}{2}}\left(\sigma_x, \sigma_y, \sigma_{xy}\right)zdz. \tag{10}$$

Substituting Eq. (9) into Eq. (10) taking into account Eqs. (6, 7), we have

$$\begin{bmatrix}N_x\\ N_y\\ N_{xy}\\ M_x\\ M_y\\ M_{xy}\end{bmatrix}=\begin{bmatrix}B_{11} & B_{12} & 0 & C_{11} & C_{12} & 0\\ B_{12} & B_{22} & 0 & C_{12} & C_{22} & 0\\ 0 & 0 & B_{66} & 0 & 0 & C_{66}\\ C_{11} & C_{12} & 0 & F_{11} & F_{12} & 0\\ C_{12} & C_{22} & 0 & F_{12} & F_{22} & 0\\ 0 & 0 & C_{66} & 0 & 0 & F_{66}\end{bmatrix}\begin{bmatrix}\varepsilon_x^0\\ \varepsilon_y^0\\ \gamma_{xy}^0\\ -\chi_x\\ -\chi_y\\ -2\chi_{xy}\end{bmatrix}-\begin{bmatrix}\Phi_{1x}^T\\ \Phi_{1y}^T\\ 0\\ \Phi_{2x}^T\\ \Phi_{2y}^T\\ 0\end{bmatrix}, \tag{11}$$

where B_{ij}, C_{ij}, F_{ij} are components of stiffness matrix of shell.

From Eq. (11) we get the relation

$$\begin{aligned}
\varepsilon_x^0 &= B_{22}^* N_x - B_{12}^* N_y + C_{11}^* \chi_x + C_{12}^* \chi_y + B_{22}^* \phi_{1x}^T - B_{12}^* \phi_{1y}^T, \\
\varepsilon_y^0 &= B_{11}^* N_y - B_{12}^* N_x + C_{21}^* \chi_x + C_{22}^* \chi_y - B_{12}^* \phi_{1x}^T + B_{11}^* \phi_{1y}^T, \\
\gamma_{xy}^0 &= N_{xy} B_{66}^* + 2C_{66}^* \chi_{xy},
\end{aligned} \tag{12}$$

in which

$$\begin{aligned}
&B_{11}^* = \frac{B_{11}}{\Delta}, B_{22}^* = \frac{B_{22}}{\Delta}, B_{12}^* = \frac{B_{12}}{\Delta}, B_{66}^* = \frac{1}{B_{66}}, \\
&C_{11}^* = B_{22}^* C_{11} - B_{12}^* C_{12}, C_{22}^* = B_{11}^* C_{22} - B_{12}^* C_{12}, \\
&C_{12}^* = B_{22}^* C_{12} - B_{12}^* C_{22}, C_{21}^* = B_{11}^* C_{12} - B_{12}^* C_{11}, \\
&C_{66}^* = \frac{C_{66}}{B_{66}}, \Delta = B_{11} B_{22} - B_{12}^2.
\end{aligned} \tag{13}$$

Combining Eq. (11) and (12) leads to

$$\begin{aligned}
M_x &= C_{11}^* N_x + C_{21}^* N_y - F_{11}^* \chi_x - F_{12}^* \chi_y + F_{14}^* \phi_{1x}^T + F_{24}^* \phi_{1y}^T - \phi_{2x}^T, \\
M_y &= C_{12}^* N_x + C_{22}^* N_y - F_{21}^* \chi_x - F_{22}^* \chi_y + F_{15}^* \phi_{1x}^T + F_{25}^* \phi_{1y}^T - \phi_{2y}^T, \\
M_{xy} &= C_{66}^* N_{xy} - 2F_{66}^* \chi_{xy},
\end{aligned} \tag{14}$$

where

$$\begin{aligned}
&F_{11}^* = F_{11} - C_{11} C_{11}^* - C_{12} C_{21}^*,\ F_{22}^* = F_{22} + C_{12} C_{12}^* - C_{22} C_{22}^*, \\
&F_{12}^* = F_{12} - C_{11} C_{12}^* - C_{12} C_{22}^*,\ F_{21}^* = F_{12} - C_{12} C_{11}^* - C_{22} C_{21}^*, \\
&F_{66}^* = F_{66} - C_{66} C_{66}^*,\ F_{14}^* = C_{11} B_{22}^* - C_{12} B_{12}^*,\ F_{24}^* = C_{12} B_{11}^* - C_{11} B_{12}^*, \\
&F_{15}^* = C_{12} B_{22}^* - C_{22} B_{12}^*,\ F_{25}^* = C_{22} B_{11}^* - C_{12} B_{12}^*.
\end{aligned} \tag{15}$$

The equilibrium equations of FG-GRC laminated cylindrical shell taking into account two-parameter Pasternak's elastic foundations based on the Donnell shell theory are presented as

$$\begin{aligned}
&N_{x,x} + N_{xy,y} = 0, \\
&N_{xy,x} + N_{y,y} = 0, \\
&M_{x,xx} + 2M_{xy,xy} + M_{y,yy} + N_x w_{,xx} + 2N_{xy} w_{,xy} \\
&\qquad + N_y w_{,yy} + \frac{N_y}{R} - K_1 w + K_2 \left(w_{,xx} + w_{,yy} \right) = 0.
\end{aligned} \tag{16}$$

Introducing Airy's stress function $\varphi(x, y)$ which satisfies the following conditions

$$N_x = \varphi_{,yy}, \qquad N_y = \varphi_{,xx}, \qquad N_{xy} = -\varphi_{,xy}. \tag{17}$$

As can be seen, with the proposed Airy's stress function (17), the first two of Eq. (16) are completely satisfied. Substituting Eqs. (14) and (17) into the third equation of Eq. (16) and combining the Eqs. (6) and (7), and substituting Eqs. (17) and (12) into Eq. (8), the equilibrium and compatibility equations are rewritten by

$$\begin{aligned}
&F_{11}^* w_{,xxxx} + \left(F_{12}^* + F_{21}^* + 4F_{66}^* \right) w_{,xxyy} + F_{22}^* w_{,yyyy} - C_{21}^* \varphi_{,xxxx} - \\
&- \left(C_{11}^* + C_{22}^* - 2C_{66}^* \right) \varphi_{,xxyy} - C_{12}^* \varphi_{,yyyy} - \frac{1}{R} \varphi_{,xx} - \varphi_{,yy} w_{,xx} - \\
&\qquad - \varphi_{,xx} w_{,yy} + 2\varphi_{,xy} w_{,xy} + K_1 w - K_2 \left(w_{,xx} + w_{,yy} \right) = 0,
\end{aligned} \tag{18}$$

$$\begin{aligned}
&B_{11}^* \varphi_{,xxxx} + \left(B_{66}^* - 2B_{12}^* \right) \varphi_{,xxyy} + B_{22}^* \varphi_{,yyyy} + C_{21}^* w_{,xxxx} + \\
&+ \left(C_{11}^* + C_{22}^* - 2C_{66}^* \right) w_{,xxyy} + C_{12}^* w_{,yyyy} - w_{,xy}^2 + w_{,xx} w_{,yy} + \frac{1}{R} w_{,xx} = 0.
\end{aligned} \tag{19}$$

Nonlinear stability of FG-GRC laminated cylindrical shells under axial compression surrounded by an elastic foundation in thermal environment is analyzed by applying two nonlinear governing equations (18) and (19).

4. Boundary Condition and Galerkin Procedure

Consider an FG-GRC laminated cylindrical shell subjected to axial compression with simply supported boundary conditions at the edges. Then, the deflection of the axially loaded shell is approximately chosen in three-term form with pre-buckling deflection amplitude ξ_0, linear and nonlinear post-buckling deflection amplitudes ξ_1,ξ_2, respectively, as follows

$$w=\xi_0+\xi_1\sin\frac{m\pi x}{L}\sin\frac{ny}{R}+\xi_2\sin^2\frac{m\pi x}{L}. \tag{20}$$

Substituting the deflection form (20) into Eq. (19) to obtain the stress function form

$$\begin{aligned}\varphi=&A_1\cos\frac{2m\pi x}{L}+A_2\cos\frac{2ny}{R}-A_3\sin\frac{m\pi x}{L}\sin\frac{ny}{R}+\\&+A_4\sin\frac{3m\pi x}{L}\sin\frac{ny}{R}-\sigma_{0y}h\frac{x^2}{2}-ph\frac{y^2}{2},\end{aligned} \tag{21}$$

in which

$$\begin{aligned}&A_1=\frac{n^2\lambda^2}{32B_{11}^*m^2\pi^2}f_1^2-\frac{\left(\lambda L-4C_{21}^*m^2\pi^2\right)}{8B_{11}^*m^2\pi^2}f_2, &&A_2=\frac{m^2\pi^2}{32B_{22}^*n^2\lambda^2}f_1^2,\\&A_3=\frac{X}{V}f_1+\frac{m^2n^2\pi^2\lambda^2}{V}f_1f_2, &&A_4=\frac{m^2n^2\pi^2\lambda^2}{Z}f_1f_2,\\&V=B_{11}^*m^4\pi^4+\left(B_{66}^*-2B_{12}^*\right)m^2n^2\pi^2\lambda^2+B_{22}^*n^4\lambda^4,\\&Y=F_{11}^*m^4\pi^4+\left(F_{12}^*+F_{21}^*+4F_{66}^*\right)m^2n^2\pi^2\lambda^2+F_{22}^*n^4\lambda^4,\\&X=C_{21}^*m^4\pi^4+\left(C_{11}^*+C_{22}^*-2C_{66}^*\right)m^2n^2\pi^2\lambda^2+C_{12}^*n^4\lambda^4-\frac{L^2}{R}m^2\pi^2,\\&Z=81B_{11}^*m^4\pi^4+9\left(B_{66}^*-2B_{12}^*\right)m^2n^2\pi^2\lambda^2+B_{22}^*n^4\lambda^4, &&\lambda=\frac{L}{R}.\end{aligned}$$

Introducing deflection and stress function forms into Eq. (18). Then, the Galerkin method is applied in the ranges $0\le y\le 2\pi R$ and $0\le x\le L$ leads to

$$\sigma_{0y}h=-\frac{1}{2}RK_1\left(\xi_2+2\xi_0\right), \tag{22}$$

$$\begin{aligned}&\left(Y+\frac{X^2}{V}\right)\xi_1+\frac{1}{16}\left(\frac{m^4\pi^4}{B_{22}^*}+\frac{n^4\lambda^4}{B_{11}^*}\right)f_1^3+\\&+n^2\lambda^2\left[\frac{2Xm^2\pi^2}{V}-\frac{\left(\lambda L-4C_{21}^*m^2\pi^2\right)}{4B_{11}^*}\right]\xi_1\xi_2+\\&+m^4n^4\pi^4\lambda^4\left(\frac{1}{V}+\frac{1}{Z}\right)\xi_1\xi_2^2-m^2\pi^2L^2hp\xi_1-\\&-\sigma_{0y}hn^2L^2\lambda^2\xi_1+L^4K_1\xi_1+L^2K_2\xi_1\left[\left(\lambda n\right)^2+\left(m\pi\right)^2\right]=0,\end{aligned} \tag{23}$$

$$\begin{aligned}&\left\{\left[4C_{21}^*\left(\frac{m\pi}{L}\right)^4-\frac{1}{R}\left(\frac{m\pi}{L}\right)^2\right]\frac{n^2\lambda^2}{16B_{11}^*m^2\pi^2}+\frac{1}{2}\frac{X}{V}\left(\frac{m\pi}{L}\right)^2\left(\frac{n}{R}\right)^2\right\}\xi_1^2+\\&+\frac{1}{2}m^2n^2\pi^2\lambda^2\left(\frac{m\pi}{L}\right)^2\left(\frac{n}{R}\right)^2\left(\frac{1}{V}-\frac{1}{Z}\right)\xi_1^2\xi_2+\\&+\left\{4F_{11}^*\left(\frac{m\pi}{L}\right)^4-\left[4C_{21}^*\left(\frac{m\pi}{L}\right)^4-\frac{1}{R}\left(\frac{m\pi}{L}\right)^2\right]\frac{\lambda L-4C_{21}^*m^2\pi^2}{4B_{11}^*m^2\pi^2}\right\}\xi_2+\\&-ph\left(\frac{m\pi}{L}\right)^2\xi_2+\frac{\sigma_{0y}h}{R}+K_1\left(\frac{3}{4}\xi_2+\xi_0\right)+K_2\xi_2\left(\frac{m\pi}{L}\right)^2=0,\end{aligned} \tag{24}$$

Circumferential closed condition must be satisfied for a cylindrical shell

$$\int_0^{2\pi R}\int_0^L v_{,y}dxdy=\int_0^{2\pi R}\int_0^L\left[\varepsilon_y^0+\frac{w}{R}-\frac{1}{2}w_{,x}^2\right]dxdy=0. \tag{25}$$

By combining Eqs. (12), (17) and (20), the integral (25) leads to

$$-2B_{11}^*\sigma_{0y}h+2B_{12}^*ph+\frac{1}{R}(\xi_2+2\xi_0)-\frac{1}{4}\left(\frac{n}{R}\right)^2\xi_1^2+2\left(-B_{12}^*\phi_{1x}^T+B_{11}^*\phi_{1y}^T\right)=0. \tag{26}$$

Substituting σ_{0y} in Eq. (22) into Eqs. (23, 24) and the circumferential closed condition (26), equilibrium equation system (23-24, 26) is written by

$$\xi_0=\frac{U_{32}}{2U_{31}}\xi_1^2-\frac{U_{34}}{2U_{31}}p-\frac{1}{2}\xi_2-\frac{U_{35}}{2U_{31}}, \tag{27}$$

$$U_{11}+U_{12}\xi_0+U_{13}\xi_1^2+U_{14}\xi_2+U_{15}\xi_2^2-U_{16}p=0, \tag{28}$$

$$\xi_1^2=\frac{U_{24}\xi_2p-U_{23}\xi_2}{U_{21}+U_{22}\xi_2}, \tag{29}$$

where

$$U_{11}=\left(Y+\frac{X^2}{V}\right)+L^4K_1+L^2K_2\left[(\lambda n)^2+(m\pi)^2\right],\ U_{12}=n^2L^2\lambda^2RK_1,$$

$$U_{13}=\frac{1}{16}\left(\frac{m^4\pi^4}{B_{22}^*}+\frac{n^4\lambda^4}{B_{11}^*}\right),\ U_{14}=\frac{2Xm^2n^2\pi^2\lambda^2}{V}-\frac{n^2\lambda^2\left(\lambda L-4C_{21}^*m^2\pi^2\right)}{4B_{11}^*}+\frac{1}{2}n^2L^2\lambda^2RK_1,$$

$$U_{15}=\left(\frac{m^4n^4\pi^4\lambda^4}{V}+\frac{m^4n^4\pi^4\lambda^4}{Z}\right),\ U_{16}=m^2\pi^2L^2h,$$

$$U_{21}=\left\{\left[4C_{21}^*\left(\frac{m\pi}{L}\right)^4-\frac{1}{R}\left(\frac{m\pi}{L}\right)^2\right]\frac{n^2\lambda^2}{16B_{11}^*m^2\pi^2}+\frac{1}{2}\frac{X}{V}\left(\frac{m\pi}{L}\right)^2\left(\frac{n}{R}\right)^2\right\},$$

$$U_{22}=\frac{1}{2}m^2n^2\pi^2\lambda^2\left(\frac{m\pi}{L}\right)^2\left(\frac{n}{R}\right)^2\left(\frac{1}{V}-\frac{1}{Z}\right),\ U_{24}=h\left(\frac{m\pi}{L}\right)^2,$$

$$U_{23}=\left\{4F_{11}^*\left(\frac{m\pi}{L}\right)^4-\left[4C_{21}^*\left(\frac{m\pi}{L}\right)^4-\frac{1}{R}\left(\frac{m\pi}{L}\right)^2\right]\frac{\lambda L-4C_{21}^*m^2\pi^2}{4B_{11}^*m^2\pi^2}+\frac{1}{4}K_1+K_2\left(\frac{m\pi}{L}\right)^2\right\},$$

$$U_{31}=\left(B_{11}^*RK_1+\frac{1}{R}\right),\ U_{32}=\frac{1}{4}\left(\frac{n}{R}\right)^2,\ U_{34}=2B_{12}^*h,\ U_{35}=2\left(-B_{12}^*\phi_{1x}^T+B_{11}^*\phi_{1y}^T\right).$$

Substituting $\xi_{0,}$ ξ_1^2 from Eqs. (27) and (29) into Eq. (28) leads to

$$p=\left(U_{11}+U_{14}\xi_2-U_{12}\frac{1}{2}\xi_2-U_{12}\frac{U_{35}}{2U_{13}}+U_{15}\xi_2^2-U_{12}\frac{U_{32}}{2U_{31}}\frac{U_{23}\xi_2}{U_{21}+U_{22}\xi_2}-\right.$$
$$\left.-\frac{U_{13}U_{23}\xi_2}{U_{21}+U_{22}\xi_2}\right)\left(-U_{12}\frac{U_{32}}{2U_{31}}\frac{U_{24}\xi_2}{U_{21}+U_{22}\xi_2}-\frac{U_{13}U_{24}\xi_2}{U_{21}+U_{22}\xi_2}+U_{16}+U_{12}\frac{U_{34}}{2U_{31}}\right)^{-1}. \tag{30}$$

When $\xi_2\to 0$, the upper axial compressive buckling load of FG-GRC laminated cylindrical shells is received from Eq. (30), as follow:

$$p_{upper}=\left(U_{11}-U_{12}\frac{U_{35}}{2U_{13}}\right)/\left(U_{16}+U_{12}\frac{U_{34}}{2U_{31}}\right). \tag{31}$$

Critical axial compressive buckling load p_{cr} of FG-GRC laminated cylindrical shells is the minimal value of upper buckling axial compressive loads p_{upper} vs. (m,n).

From Eq. (20), the maximal deflection of the shells is determined by

$$W_{\max} = \xi_0 + \xi_1 + \xi_2, \tag{32}$$

locates at $x = \dfrac{iL}{2m}$, $y = \dfrac{j\pi R}{2n}$ where i, j are odd integer numbers.

Substituting Eqs. (27) and (29) into Eq. (32), the maximal deflection is rewritten respected to ξ_2

$$W_{\max} = \frac{U_{32}}{2U_{31}}\frac{U_{24}\xi_2 p - U_{23}\xi_2}{U_{21} + U_{22}\xi_2} - \frac{U_{34}}{2U_{31}}p + \frac{1}{2}\xi_2 - \frac{U_{35}}{2U_{31}} + \left(\frac{U_{24}\xi_2 p - U_{23}\xi_2}{U_{21} + U_{22}\xi_2}\right)^{1/2}. \tag{33}$$

The average end-shortening ratio $\bar{\Delta}_x$ are taken as:

$$\bar{\Delta}_x = -\frac{1}{2\pi RL}\int_0^{2\pi R}\int_0^L u_{,x}dxdy = -\frac{1}{2\pi RL}\int_0^{2\pi R}\int_0^L \left(\varepsilon_x^0 - \frac{1}{2}w_{,x}^2\right)dxdy. \tag{34}$$

By using Eqs. (12), (17) and (20), Eq. (34) becomes

$$\bar{\Delta}_x = B_{22}^* ph - B_{12}^*\sigma_{oy}h + \frac{1}{4}\left(\frac{m\pi}{L}\right)^2\xi_2^2 + \frac{1}{8}\left(\frac{m\pi}{L}\right)^2\xi_1^2 - \left(B_{22}^*\phi_{1x}^T - B_{12}^*\phi_{1y}^T\right). \tag{35}$$

By combining Eq. (22) and Eqs. (27-29), we have

$$\begin{aligned}\bar{\Delta}_x = {} & B_{22}^* ph + \frac{1}{2}B_{12}^* RK_1\xi_2 + B_{12}^* RK_1\left(\frac{U_{32}}{2U_{31}}\frac{U_{24}\xi_2 p - U_{23}\xi_2}{U_{21} + U_{22}\xi_2} - \frac{U_{34}}{2U_{31}}p - \right.\\ & \left. -\frac{1}{2}\xi_2 - \frac{U_{35}}{2U_{31}}\right) + \frac{1}{4}\left(\frac{m\pi}{L}\right)^2\xi_2^2 + \frac{1}{8}\left(\frac{m\pi}{L}\right)^2\frac{U_{24}\xi_2 p - U_{23}\xi_2}{U_{21} + U_{22}\xi_2} - \left(B_{22}^*\phi_{1x}^T - B_{12}^*\phi_{1y}^T\right).\end{aligned} \tag{36}$$

When $\xi_1, \xi_2 \to 0$, the average end shortening ratio expression of prebuckling state is obtained as

$$\bar{\Delta}_x = B_{22}^* ph - B_{12}^* RK_1\left(\frac{U_{34}}{2U_{31}}p + \frac{U_{35}}{2U_{31}}\right) - \left(B_{22}^*\phi_{1x}^T - B_{12}^*\phi_{1y}^T\right). \tag{37}$$

As can be seen in Eq. (37), in prebuckling state the relationship between $\bar{\Delta}_x$ and p is linear. Combining Eq. (29) with Eqs. (33) and (36), the static postbuckling load-maximal deflection and load-average end shortening postbuckling curves of shells can be numerically investigated, respectively.

5. Numerical Results and Discussions

5.1 Comparison results

Comparisons of the critical axial compressive buckling load p_{cr} of FG-GRC laminated cylindrical shells with different geometrical parameters with the work of Shen and Xiang [34] are shown in Table 2. Two types of UD and FG-X distribution of each sample with different geometrical parameters were compared. Then, the present result of $p - \bar{\Delta}_x$ post-buckling curve of isotropic cylindrical shell subjected to axial compression is compared with the results of Shen [12], Huang and Han [16] and Yamaki [39] in Fig. 2. The results in Table 2 and Fig. 2 show that the very good agreements are obtained.

Table 2. Comparisons of critical axial compressive buckling load p_{cr} (in kN) of FG-GRC laminated cylindrical shells with different geometric dimensions ($R/h = 20$, $h = 2\ mm$, $T = 300K$).

L^2/Rh	Sample shell	Shen and Xiang [34]		Present	
		UD	FG-X	UD	FG-X
100	$(0)_{10}$	1056.72 (2;4)*	1116.33 (2;4)	1107.81 (2;4)	1194.79 (2;4)
	$(0/90/0/90/0)_S$	1057.20 (2;4)	1116.70 (2;4)	1108.20 (2;4)	1194.88 (2;4)
	$(0/90)_{5T}$	1057.66 (2;4)	1117.73 (2;4)	1108.67 (2;4)	1196.04 (2;4)
300	$(0)_{10}$	1098.08 (3;4)	1167.68 (3;4)	1143.80 (3;4)	1238.44 (3;4)
	$(0/90/0/90/0)_S$	1098.87 (3;4)	1168.23 (3;4)	1144.63 (3;4)	1238.95 (3;4)
	$(0/90)_{5T}$	1099.57 (3;4)	1169.80 (3;4)	1145.39 (3;4)	1240.73 (3;4)
500	$(0)_{10}$	1087.11 (4;4)	1154.36 (4;4)	1133.55 (4;4)	1226.10 (4;4)
	$(0/90/0/90/0)_S$	1087.81 (4;4)	1154.83 (4;4)	1134.25 (4;4)	1226.49 (4;4)
	$(0/90)_{5T}$	1088.45 (4;4)	1156.27 (4;4)	1134.94 (4;4)	1228.12 (4;4)

* The numbers in the parentheses denote the buckling mode ($m;n$).

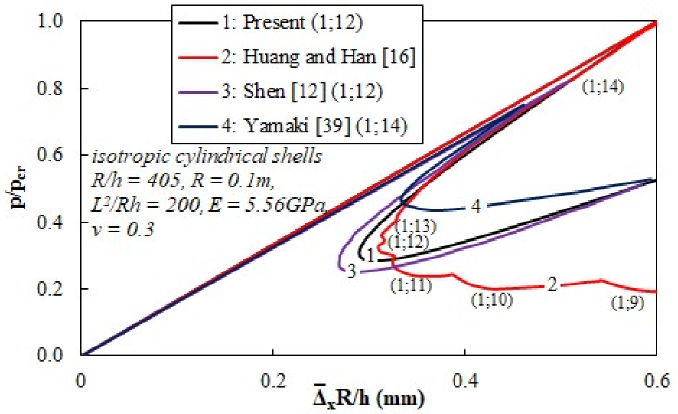

Fig. 2. Comparison of the $p-\bar{\Delta}_x$ postbuckling curves of isotropic cylindrical shell subjected to axial compression

5.2 Material parameters

In this section, the material and geometrical parameters of considered FG-GRC laminated cylindrical shells are given by $L = 0.09m$, $R/h = 20$, $K_1 = 2.5\times10^7\ N/m^3$ and $K_2 = 2.5\times10^5\ N/m$.

The total thickness of FG-GRC laminated cylindrical shells is $h = 2mm$ which includes ten layers with $0.2mm$ for each layer. The geometrical parameters of the graphene sheets are taken in the report of Shen and Xiang [34] (Eqs. (1) and (2)) as follows $a_G = 14.76nm$, $b_G = 14.77nm$ and $h_G = 0.188nm$. The performance parameters of each GRC layer are determined in Table 1.

In Table 1, the temperature-dependent material parameters are applied into Eq. (1). Based on the Eq. (31) with various combinations of the buckling modes $(m;\ n)$ the critical axial compressive buckling load of FG-GRC laminated cylindrical shell can be found.

5.3 Effect of uniform environment temperature *T*

Table 3 shows the effects of environmental temperature T on the critical axial compressive buckling load p_{cr} of FG-GRC laminated cylindrical shells. As can be seen, a sample of cylindrical shell lightly influences to the critical axial compressive buckling load, conversely, environment temperature and distribution type of graphene reinforced layers strongly influence on the critical axial compressive buckling load of shells. Critical buckling load of shell decreases when the environment temperature increases. Also, the critical buckling load of the shell is the largest with FG-X distribution type and smallest with FG-O distribution type.

Table 3. Effects of environment temperature T on the critical axial compressive buckling load p_{cr} (GPa) of shells.

$T(K)$	Sample shell	UD	FG-X	FG-V	FG-Λ	FG-O
300	$(0)_{10}$	2.389 (4;4)	2.513 (4;3)	2.022 (4;4)	2.158 (5;3)	1.945 (4;4)
	$(0/90/0/90/0)_S$	2.389 (4;4)	2.516 (4;3)	2.021 (4;4)	2.159 (5;3)	1.944 (4;4)
	$(0/90)_{5T}$	2.388 (4;4)	2.513 (4;3)	2.019 (4;4)	2.157 (5;3)	1.945 (4;4)
400	$(0)_{10}$	2.098 (4;4)	2.191 (4;3)	1.829 (4;4)	1.862 (4;4)	1.708 (4;4)
	$(0/90/0/90/0)_S$	2.097 (4;4)	2.194 (4;3)	1.830 (4;4)	1.862 (4;4)	1.708 (4;4)
	$(0/90)_{5T}$	2.097 (4;4)	2.191 (4;3)	1.829 (4;4)	1.860 (4;4)	1.708 (4;4)
500	$(0)_{10}$	1.944 (3;4)	2.075 (4;3)	1.763 (4;4)	1.749 (4;4)	1.620 (4;4)
	$(0/90/0/90/0)_S$	1.944 (3;4)	2.076 (4;3)	1.764 (4;4)	1.749 (4;4)	1.620 (4;4)
	$(0/90)_{5T}$	1.944 (3;4)	2.074 (4;3)	1.763 (4;4)	1.748 (4;4)	1.620 (4;4)

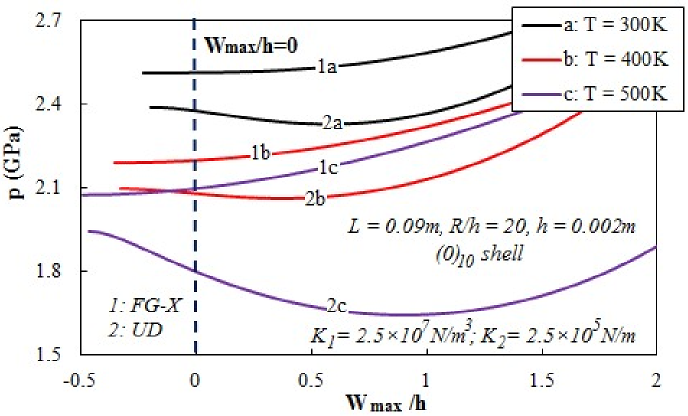

Fig. 3. Effect of environment temperature on $p-W_{\max}/h$ postbuckling curves of $(0)_{10}$ cylindrical shells

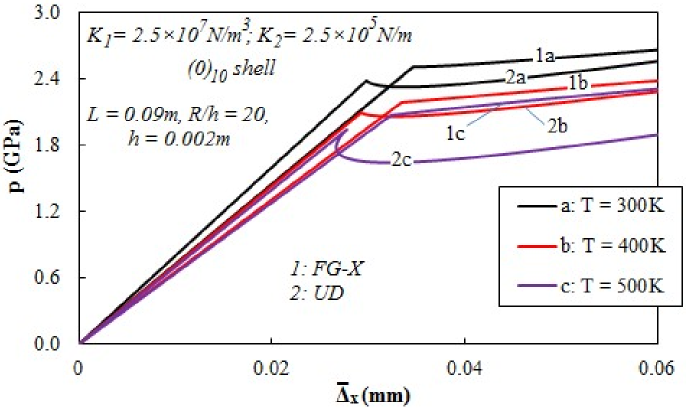

Fig. 4. Effect of environment temperature on $p-\bar{\Delta}_x$ postbuckling curves of $(0)_{10}$ cylindrical shells

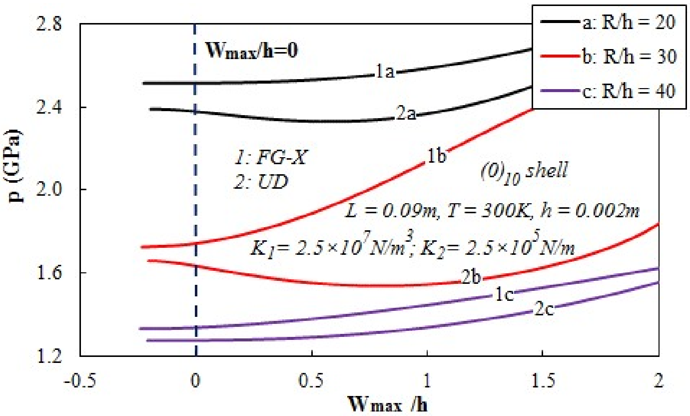

Fig. 5. Effect of R/h ratio on $p-W_{max}/h$ postbuckling curves

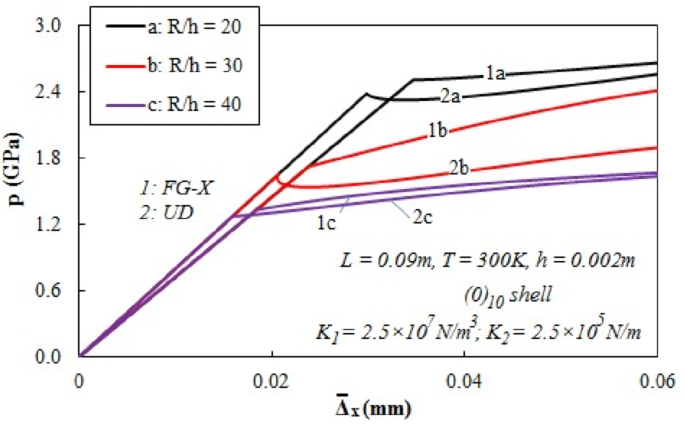

Fig. 6. Effect of R/h ratio on $p-\bar{\Delta}_x$ postbuckling curves

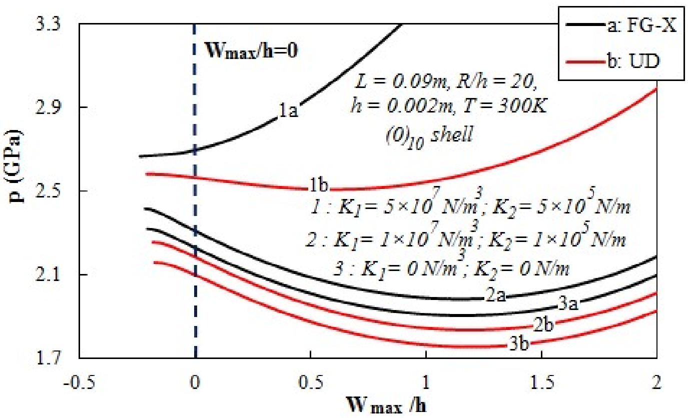

Fig. 7. Effect of elastic foundations on $p-W_{max}/h$ postbuckling curves

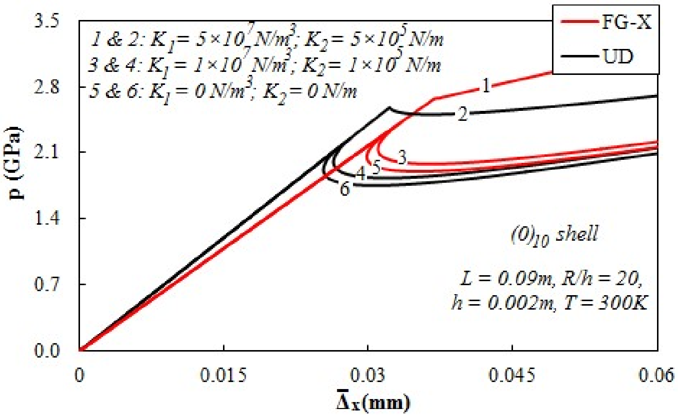

Fig. 8. Effect of elastic foundations on $p-\bar{\Delta}_x$ postbuckling curves

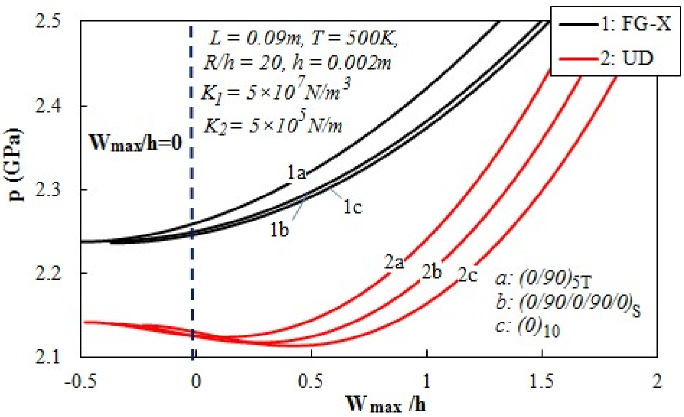

Fig. 9. Effect of GRC distribution type on $p-W_{\max}/h$ postbuckling curves

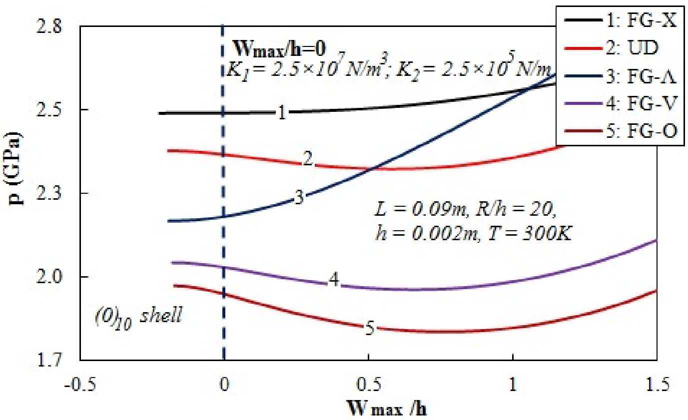

Fig. 10. Effect of GRC distribution type of (0)10 shell on $p-W_{\max}/h$ postbuckling curves

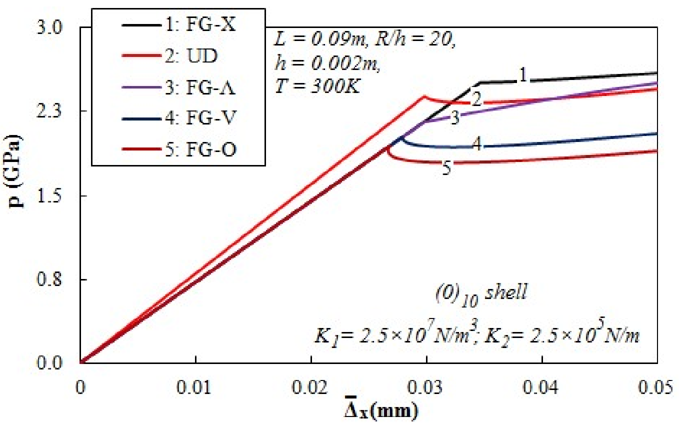

Fig. 11. Effect of GRC distribution type of (0)10 shell on $p-\bar{\Delta}_x$ postbuckling curves

Effects of environment temperature on the $p - W_{\max}/h$ and $p - \bar{\Delta}_x$ post-buckling curves with the critical buckling mode of UD and FG-X type of $(0)_{10}$ cylindrical shells are shown in Figs. 3 and 4. As can be observed, the complex behavior of nonlinear post-buckling curves is obtained. In addition, post-buckling curves of FG-X cylindrical shells are upper than one of UD cylindrical shells, post-buckling curve of FG-GRC cylindrical shells is upper with lesser of environment temperature, respectively. Snap-through phenomenon is clearly observed with UD distribution type, contrary, it is not observed with FG-X distribution type in all numerical investigations.

5.4 Effect of geometric dimensions R/h

Effect of R/h ratio and graphene distribution type on the critical axial compressive buckling load of FG-GRC cylindrical shell are investigated in table 4. Clearly, R/h ratio of shells significantly influences on the critical axial compressive buckling load. In addition, effects of R/h ratio on the $p - W_{\max}/h$ and $p - \bar{\Delta}_x$ nonlinear post-buckling curves are presented in Figs. 5 and 6. Due to complex behavior of FG-GRC cylindrical shell, the irregular changes on post-buckling curve are obtained when the R/h ratio varies.

Table 4. Effect of R/h ratio of shells on critical axial compressive buckling load p_{cr} (GPa)

Sample shell	*UD*	*FG-X*	*FG-V*	*FG-Λ*	*FG-O*
			$R/h = 20$		
$(0)_{10}$	2.389 (4;4)	2.513 (4;3)	2.022 (4;4)	2.158 (5;3)	1.945 (4;4)
$(0/90/0/90/0)_S$	2.389 (4;4)	2.516 (4;3)	2.021 (4;4)	2.159 (5;3)	1.944 (4;4)
$(0/90)_{5T}$	2.388 (4;4)	2.513 (4;3)	2.019 (4;4)	2.157 (5;3)	1.945 (4;4)
			$R/h = 30$		
$(0)_{10}$	1.660 (3;5)	1.726 (4;3)	1.415 (4;4)	1.485 (5;1)	1.352 (4;4)
$(0/90/0/90/0)_S$	1.659 (3;5)	1.728 (4;3)	1.414 (4;4)	1.485 (5;1)	1.351 (4;4)
$(0/90)_{5T}$	1.659 (3;5)	1.725 (4;3)	1.412 (4;4)	1.483 (5;1)	1.352 (4;4)
			$R/h = 40$		
$(0)_{10}$	1.277 (3;5)	1.333 (3;4)	1.101 (3;5)	1.146 (4;2)	1.054 (4;4)
$(0/90/0/90/0)_S$	1.277 (3;5)	1.335 (3;4)	1.101 (3;5)	1.146 (4;2)	1.052 (4;4)
$(0/90)_{5T}$	1.276 (3;5)	1.334 (3;4)	1.100 (3;5)	1.145 (4;2)	1.053 (4;4)

5.5 Effect of elastic foundation parameters

Table 5, Figs. 7 and 8 show the effects of Pasternak elastic foundation parameters on the critical axial compressive buckling load and post-buckling curve of FG-GRC cylindrical shells, respectively. As can be observed, the elastic foundation parameters strongly influence on the critical buckling load and post-buckling behavior of shells. The results confirm that the snap-through phenomenon is more clearly observed with smaller values of elastic foundation parameters.

Table 5. Effect of elastic foundation parameters of shells on the critical axial compressive buckling load p_{cr} (GPa)

Sample shell	*UD*	*FG-X*	*FG-V*	*FG-Λ*	*FG-O*
		$K_1 = 0\,N/m^3$, $K_2 = 0\,N/m$			
$(0)_{10}$	2.156 (3;4)	2.317 (3;4)	1.815 (3;4)	1.991 (3;4)	1.755 (2;4)
$(0/90/0/90/0)_S$	2.156 (3;4)	2.317 (3;4)	1.815 (3;4)	1.990 (3;4)	1.754 (4;4)
$(0/90)_{5T}$	2.156 (3;4)	2.317 (3;4)	1.815 (3;4)	1.990 (4;4)	1.755 (4;4)
		$K_1 = 1\times10^7\,N/m^3$, $K_2 = 1\times10^5\,N/m$			
$(0)_{10}$	2.252 (3;4)	2.413 (3;4)	1.908 (4;4)	2.067 (4;4)	1.831 (4;4)
$(0/90/0/90/0)_S$	2.252 (3;4)	2.413 (3;4)	1.907 (4;4)	2.067 (4;4)	1.830 (4;4)
$(0/90)_{5T}$	2.252 (3;4)	2.413 (3;4)	1.906 (4;4)	2.066 (4;4)	1.831 (4;4)
		$K_1 = 5\times10^7\,N/m^3$, $K_2 = 5\times10^5\,N/m$			
$(0)_{10}$	2.579 (4;4)	2.663 (5;2)	2.205 (5;3)	2.289 (6;1)	2.110 (5;3)
$(0/90/0/90/0)_S$	2.578 (4;4)	2.667 (5;2)	2.204 (5;3)	2.289 (6;1)	2.109 (5;3)
$(0/90)_{5T}$	2.577 (4;4)	2.663 (5;2)	2.201 (5;3)	2.286 (6;1)	2.110 (5;3)

5.6 Effects of GRCs distribution

Fig. 9 presents the postbuckling curves of $(0/90)_{5T}$, $(0/90/0/90/0)_S$ and $(0)_{10}$ FG-GRC cylindrical shells. Two considered types of graphene distribution are FG-X and UD types. Figs. 10-13 investigate the effects of GRC distribution type of $(0)_{10}$ and $(0/90)_{5T}$ shell on $p - W_{\max}/h$ and $p - \bar{\Delta}_x$ postbuckling curves. As can be seen in all numerical investigations, postbuckling curve of FG-Λ cylindrical shell is lower than those of FG-X and UD cylindrical shell with small deflection, however, postbuckling curve of FG-Λ cylindrical shell is upper than those of FG-X and UD cylindrical shell when the deflection is sufficiently large. Snap-through phenomenon is not obtained with FG-X and FG-Λ cylindrical shells.

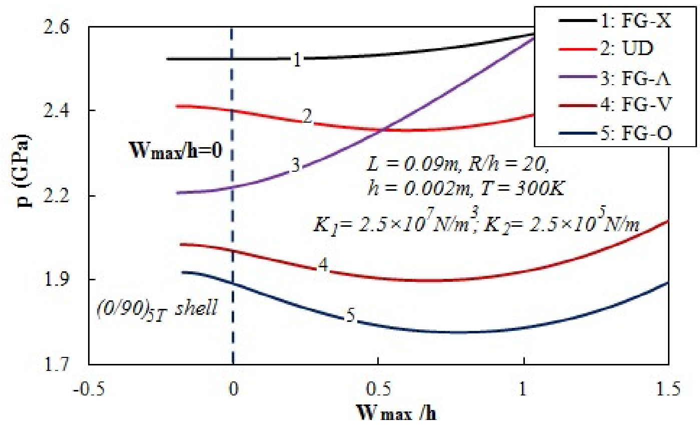

Fig. 12. Effect of GRC distribution type of (0/90)$_{5T}$ shell on $p - W_{\max}/h$ postbuckling curves

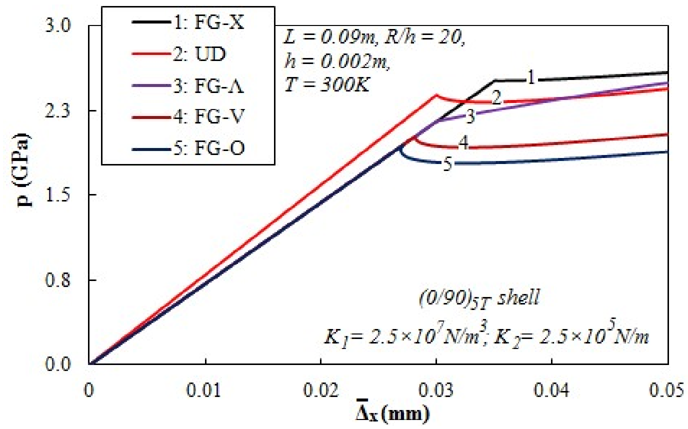

Fig. 13. Effect of GRC distribution type of (0/90)$_{5T}$ shell on $p - \bar{\Delta}_x$ postbuckling curves

6. Conclusions

An analytical approach of nonlinear buckling and postbuckling behavior of FG-GRC laminated cylindrical shells under axial compressive load surrounded by elastic foundations in thermal environment by using a simple and effective calculation procedure was presented in this paper. The properties and parameters of material depend on the temperature which were taken according to Halpin-Tsai micromechanical model. Five types of each application with three sample shells were considered in the paper. Numerical results showed that the load carrying-capacity of FG-X is better than that of other types. Some significant remarks are obtained as follows:

i. The distribution of GRCs significantly influences on the critical axial compressive buckling load.

ii. Temperature, geometrical properties, elastic foundations, volume fraction index strongly influence to the load-carrying capacity of FG-GRC laminated cylindrical shells.

iii. The snap-through phenomenon is more clearly observed with UD, FG-V and FG-O types, a converse behavior is obtained with FG-X and FG-Λ types.

iv. Postbuckling curves of shells irregularly vary when the environment temperature, geometrical properties and material properties vary.

Conflict of Interest

The authors declared no potential conflicts of interest with respect to the research, authorship and publication of this article.

Funding

The authors received no financial support for the research, authorship and publication of this article.

References

[1] Shen, H.S., Zhou P., Chen, T.Y., Postbuckling analysis of stiffened cylindrical shells under combined external pressure and axial compression, *Thin-Walled Structures*, 15(1), 1993, 43–63.

[2] Reddy, J.N., Starnes, J.H., General buckling of stiffened circular cylindrical shells according to a layerwise theory,

Computers & Structures, 49(4), 1993, 605–616.
[3] Shen, H.S, Post-buckling analysis of imperfect stiffened laminated cylindrical shells under combined external pressure and axial compression, *Computers & Structures*, 63(2), 1997, 335–348.
[4] Mandal, P., Calladine, C.R., Buckling of thin cylindrical shells under axial compression, *International Journal of Solids and Structures*, 37(33), 2000, 4509–4525.
[5] Lancaster, E.R., Calladine, C.R., Palmer, S.C., Paradoxical buckling behaviour of a thin cylindrical shell under axial compression, *International Journal of Mechanical Sciences*, 42(5), 2000, 843–865.
[6] Karagiozova, D., Jones, N., On dynamic buckling phenomena in axially loaded elastic–plastic cylindrical shells, *International Journal of Non-Linear Mechanics*, 37(7), 2002, 1223–1238.
[7] Zeng, T., Wu, L., Post-buckling analysis of stiffened braided cylindrical shells under combined external pressure and axial compression, *Composite Structures*, 60(4), 2003, 455–466.
[8] Biagi, M., Del Medico, F., Reliability-based knockdown factors for composite cylindrical shells under axial compression, *Thin-Walled Structures*, 46(12), 2008, 1351–1358.
[9] Tafreshi, A., Instability of delaminated composite cylindrical shells under combined axial compression and bending, *Composite Structures*, 82(3), 2008, 422–433.
[10] Li, Z.M., Yang, D.Q., Postbuckling of shear deformable stiffened anisotropic laminated cylindrical shell under axial compression, *Ocean Engineering*, 38(10), 2011, 1246–1255.
[11] Cao, X.T., Zhang, Z.Y., Hua, H.X., Free vibration of circular cylindrical shell with constrained layer damping, *Applied Mathematics and Mechanics*, 32, 2011, 495–506.
[12] Shen, H.S., Postbuckling analysis of axially-loaded functionally graded cylindrical shells in thermal environments, *Composites Science and Technology*, 62(7-8), 2002, 977–987.
[13] Sofiyev, A.H., Schnack, E., The stability of functionally graded cylindrical shells under linearly increasing dynamic torsional loading, *Engineering Structures*, 26(10), 2004, 1321–1331.
[14] Li, S.L., Batra, R.C., Buckling of axially compressed thin cylindrical shells with functionally graded middle layer, *Thin-Walled Structures*, 44(10), 2006, 1039–1047.
[15] Huang, H., Han, Q., Buckling of imperfect functionally graded cylindrical shells under axial compression, *European Journal of Mechanics - A/Solids*, 27(6), 2008, 1026–1036.
[16] Huang, H., Han, Q., Nonlinear elastic buckling and postbuckling of axially compressed functionally graded cylindrical shells, *International Journal of Mechanical Sciences*, 51(7), 2009, 500–507.
[17] Dung, D.V., Nam, V.H., Nonlinear dynamic analysis of eccentrically stiffened functionally graded circular cylindrical thin shells under external pressure and surrounded by an elastic medium, *European Journal of Mechanics - A/Solids*, 46, 2014, 42–53.
[18] Bich, D.H., Dung, D.V., Nam, V.H., Phuong, N.T., Nonlinear static and dynamic buckling analysis of imperfect eccentrically stiffened functionally graded circular cylindrical thin shells under axial compression, *International Journal of Mechanical Science*, 74, 2013, 190–200.
[19] Phuong, N.T., Luan, D.T., Nam, V.H., Hieu, P. T., Nonlinear approach on torsional buckling and postbuckling of functionally graded cylindrical shells reinforced by orthogonal and spiral stiffeners in thermal environment, *Proceedings of the Institution of Mechanical Engineers, Part C: Journal of Mechanical Engineering Science*, 233(6), 2019, 2091–2106.
[20] Nam, V.H., Phuong, N.T., Minh, K.V., Hieu, P.T., Nonlinear thermo-mechanical buckling and post-buckling of multilayer FGM cylindrical shell reinforced by spiral stiffeners surrounded by elastic foundation subjected to torsional loads, *European Journal of Mechanics - A/Solids*, 72, 2018, 393–406.
[21] Mehditabar, A., Rahimi, G.H., Ansari Sadrabadi, S., Three-dimensional magneto-thermo-elastic analysis of functionally graded cylindrical shell, *Applied Mathematics and Mechanics*, 38, 2017, 479–494.
[22] Sofiyev, A.H., Hui D., On the vibration and stability of FGM cylindrical shells under external pressures with mixed boundary conditions by using FOSDT, *Thin-Walled Structures*, 134, 2019, 419-427.
[23] Song, Z.G., Yang, T.Z., Liew, K.M., Active vibration control of CNT-reinforced composite cylindrical shells via piezoelectric patches, *Composite Structures*, 158, 2016, 92–100.
[24] Song, Z.G., Yang, T.Z., Liew, K.M., Vibration analysis of CNT-reinforced functionally graded composite cylindrical shells in thermal environments, *International Journal of Mechanical Sciences*, 115–116, 2016, 339–347.
[25] Hosseini, H., Kolahchi, R., Seismic response of functionally graded-carbon nanotubes-reinforced submerged viscoelastic cylindrical shell in hygrothermal environment, *Physica E: Low-dimensional Systems and Nanostructures*, 102, 2018, 101–109.
[26] Mirzaei, M., Kiani, Y., Enhancement of non-linear thermal stability of temperature dependent laminated beams with graphene reinforcements, *Composite Structures*, 186, 2018, 114–122.
[27] Mirzaei, M., Kiani, Y., Isogeometric thermal buckling analysis of temperature dependent FG graphene reinforced laminated plates using NURBS formulation, *Composite Structures*, 180, 2017, 606–616.
[28] Kiani, Y., Isogeometric large amplitude free vibration of graphene reinforced laminated plates in thermal environment using NURBS formulation, *Computer Methods in Applied Mechanics and Engineering*, 332, 2018, 86–101.
[29] Kiani, Y., NURBS-based isogeometric thermal postbuckling analysis of temperature dependent graphene reinforced composite laminated plates, *Thin-Walled Structures*, 125, 2018, 211–219.
[30] Kiani, Y., Buckling of functionally graded graphene reinforced conical shells under external pressure in thermal environment, *Composites Part B: Engineering*, 156, 2019, 128–137.

[31] Shen, H.S., Xiang, Y., Lin, F., Thermal buckling and postbuckling of functionally graded graphene-reinforced composite laminated plates resting on elastic foundations, *Thin-Walled Structures*, 118, 2017, 229–237.
[32] Shen, H.S., Xiang, Y., Lin, F., Nonlinear vibration of functionally graded graphene-reinforced composite laminated plates in thermal environments, *Computer Methods in Applied Mechanics and Engineering*, 319, 2017, 175–193.
[33] Shen, H.S., Xiang, Y., Lin, F., Nonlinear bending of functionally graded graphene reinforced composite laminated plates resting on elastic foundations in thermal environments, *Composite Structures*, 170, 2017, 80–90.
[34] Shen, H.S., Xiang, Y., Postbuckling behavior of functionally graded graphene-reinforced composite laminated cylindrical shells under axial compression in thermal environments, *Computer Methods in Applied Mechanics and Engineering*, 330, 2018, 64–82.
[35] Shen, H.S., Xiang, Y., Postbuckling of functionally graded graphene-reinforced composite laminated cylindrical shells subjected to external pressure in thermal environments, *Thin-Walled Structures*, 124, 2018, 151–160.
[36] Barati, M.R., Zenkour, A.M., Vibration analysis of functionally graded graphene platelet reinforced cylindrical shells with different porosity distributions, *Mechanics of Advanced Materials and Structures*, 26(18), 2019, 1580-1588.
[37] Wang, Y., Feng, C., Zhao, Z., Yang, J., Eigenvalue buckling of functionally graded cylindrical shells reinforced with graphene platelets (GPL), *Composite Structures*, 202, 2018, 38-46.
[38] Zhenhuan, Z., Yiwen, N., Zhenzhen, T., Shengbo, Z., Jiabin, S., Xinsheng, X., Accurate nonlinear buckling analysis of functionally graded porous graphene platelet reinforced composite cylindrical shells, *International Journal of Mechanical Sciences*, 151, 2019, 537-550.
[39] Yamaki N., Elastic stability of circular cylindrical shells, *New York: NorthHolland Press*, 1984, 218–262.

ORCID iD

Ngoc Ly Le https://orcid.org/0000-0003-3594-7248
Thi Phuong Nguyen https://orcid.org/0000-0002-7629-6501
Hoai Nam Vu https://orcid.org/0000-0002-5518-6979
Thoi Trung Nguyen https://orcid.org/0000-0001-7985-6706
Minh Duc Vu https://orcid.org/0000-0001-7798-4341